Published with permission of Kluwer Academic Publishers, Dordrecht, Boston, London

Space Science Reviews 60: 317-340, 1992.

THE GALILEO DUST DETECTOR

Eberhard Grun(1), Hugo Fechtig(1), Martha S. Hanner(2), Jochen Kissel(1), Bertil-Anders Lindblad(3), Dietmar Linkert(1) Dieter Maas(1,4), Gregor E. Morfill(5), and Herbert A. Zook(6)

1 Max-Planck-lnstitut fur Kernphysik, Heidelberg, Germany.
2 Jet Propulsion Laboratory, Pasadena, California, U.S.A.
3 Lund Observatory, Lund, Sweden.
4 Kernforschungszentrum Karlsruhe, Karlsruhe, Germany.
5 Max-Planck-lnstitut fur Extraterrestrische Physik, Garching, Germany.
6 NASA Johnson Space Center, Houston, Texas, U.S.A

Abstract.

The Galileo Dust Detector is intended to provide direct observations of dust grains with masses between 10^{-19} and 10^{-9} kg in interplanetary space and in the Jovian system, to investigate their physical and dynamical properties as functions of the distances to the Sun, to Jupiter and to its satellites, to study its interaction with the Galilean satellites and the Jovian magnetosphere. Surface phenomena of the satellites (like albedo variations), which might be effects of meteoroid impacts will be compared with the dust environment. Electric charges of particulate matter in the magnetosphere and its consequences will be studied; e.g., the effects of the magnetic field on the trajectories of dust particles and fragmentation of particles due to electrostatic disruption. The investigation is performed with an instrument that measures the mass, speed, flight direction and electric charge of individual dust particles. It is a multicoincidence detector with a mass sensitivity 10^{6} times higher than that of previous in-situ experiments which measured dust in the outer solar system. The instrument weighs 4.2 kg, consumes 2.4 W, and has a normal data transmission rate of 24 bits s^{-1} in nominal spacecraft tracking mode. On December 29, 1989 the instrument was switched-on. After the instrument had been configured to flight conditions cruise science data collection started immediately. In the period to May 18, 1990 at least 168 dust impacts have been recorded. For 81 of these dust grains masses and impact speeds have been determined. First flux values are given.

1. Introduction

The Galileo Mission provides opportunity for a thorough investigation of the interplanetary dust complex and the Jovian dust environment. The scientific objectives of the Galileo dust investigation were stated in our proposal dated November 1976: "The overall objective of the proposed investigation is the exploration of the physical and dynamical properties of small dust particles (with masses between 10^{-19} and 10^{-9} kg) in the Jovian environment. The parameters to be studied include mass, speed, flight direction, and charge of individual particles. The impact rate, size distribution, angular distribution, and charge will be determined with respect to the Jovian

distance from the satellites and the magnetospheric coordinates. The primary specific objectives are:

a. to investigate the interaction of the Galilean satellites with their dust environment in order to study the relationship between dust influx on satellites and their surface properties, and to perform direct measurements of ejecta particles from the satellites;
b. to study the interaction between dust particles and magnetospheric plasma, high-energy electrons and protons, and magnetic field, to determine the relationship between dust concentrations and attenuation of the radiation belts, and to investigate the effects of the Jovian magnetic field on the trajectories of charged dust particles;
c. to investigate the influence of the Jovian gravitational field on the interplanetary dust population and to search for rings around Jupiter."

Since the approval of the Galileo Mission in 1977, two Voyager spacecraft have flown by Jupiter and have increased our knowledge about the Jovian system considerably (Burns et al., 1980; Grun et al., 1980; Morfill et al., 1980a; Showalter et al., 1987). The existence of a dust ring of μm-sized particles around Jupiter, which had previously only been suspected (Acuna and Ness, 1976; Fillius, 1976) was confirmed by photographs taken by both spacecraft (Smith et al., 1979a, b). Since in-situ dust detectors can detect local dust concentrations much better than cameras, new information on the Jovian environment can be expected.

The reduced capability of the launching system required the Galileo spacecraft to cruise through the inner Solar System for several years and to have multiply flybys of Venus and Earth before it reaches Jupiter. This prolonged interplanetary flight trajectory provides the opportunity of investigating the interplanetary dust complex in a unique way from about 0.7 to 5 AU. During this six-year long cruise measurements by the Galileo dust detector could also serve as in-ecliptic base line for the out-of-ecliptic measurements taken by the twin dust detector on the Ulysses Mission (Grun et al., 1983).

The Galileo and Ulysses dust detectors are descendants of the dust detector flown on the HEOS-2 satellite (Dietzel et al., 1973). This instrument carried out measurements in the near-Earth space and observed interesting effects of Earth's magnetosphere and the Moon on the interplanetary dust population (Hoffmann et al., 1975, 1976; Fechtig et al., 1979). All these dust detectors are based on the impact ionization phenomenon (Friichtenicht and Slattery, 1963; Fechtig et al., 1978), which provides extremely high sensitivity for recording small dust particles. Table I compares the mass sensitivities of different interplanetary dust detectors.

TABLE I

Mass sensitivities and measurement ranges of different interplanetary dust detectors. The mass thresholds refer to 20 km s^{-1} impact speed. The Pioneer 10 and 11 detectors are threshold detectors.

Spacecraft	Mass threshold	Dynamic range	Sensitive area	References
Pioneer 8/9	2×10^{-16} kg	10^2	0.010 m^2	Grun et al., 1973

Pioneer 10	2×10^{-12} kg	-	0.26 m^2	Humes et al., 1974
Pioneer 11	10^{-11} kg	-	0.26 (0.57) m^2	Humes, 1980
HEOS 2	2×10^{-19} kg	10^4	0.010 m^2	Hoffmann et al., 1975
Helios 1/2	9×10^{-18} kg	10^4	0.012 m^2	Dietzel et al., 1973
Ulysses	2×10^{-18} kg	10^6	0.10 m^2	Grun et al., 1983
Galileo	2×10^{-18} kg	10^6	0.10 m^2	This work

A team of experts has been assembled to develop, to build and to test the dust detector instrument and its data-processing system and to carry out scientific investigations based on the data. Table II lists the present principle team members and their responsibilities. A more complete account of people whose contributed significantly to the development of the Galileo dust investigation over the past years is given in the Acknowledgements.

TABLE II
Galileo Dust Detector Team

Principal investigator	Eberhard Grun
Co-investigators	Hugo Fechtig Martha S. Hanner Jochen Kissel Bertil-Anders Lindblad Gregor E. Morfill Herbert A. Zook
Project engineer	Dietmar Linkert
Electronics engineers	Gunter Baust Rainer Hofacker Gunter Matt Werner Schneider Alfred Zahlten
Data analysts	Gudrun Linkert Dieter Maas Nadeem Siddique
Clerical support	Ortrud Kress

2. Scientific Background

2.1. INTERPLANETARY DUST

Galileo's interplanetary cruise to Jupiter comprises different stages: between Earth and Venus (two times), between Earth and the asteroidal belt (three times), within the asteroidal belt, and beyond the asteroidal belt until the arrival at the planet Jupiter.

The space between the Earth and Venus was scanned by a dust detector on the Helios space probe (Grun et al., 1980, 1985a). The Helios sensor's sensitivity was similar to that of the Galileo detector. There was a large variety of new results. In agreement with the zodiacal light experiment, which was also flown on Helios, the number of interplanetary dust grains were found to vary with $r^{(-1/3)}$ (r = distance from the Sun; Leinert et al., 1981). The Helios dust detector identified two different types of interplanetary particles orbiting the Sun: particles of densities rho = 3 to 8 g cm^{-3} on low eccentric trajectories and particles of low densities (rho < 1 g cm^{-3}) orbiting on high eccentric ellipses around the Sun (Grun et al., 1980). For a general survey see McDonnell (1978) and Leinert and Grun (1990).

For dust particles outside the Earth's orbit we have the results of two dust experiments on Pioneers 10 and 11. There the mass sensitivity was considerably lower than in the Galileo experiment. The Galileo dust detector can record particles as small as 0.1 µm diameters, i.e., 2 orders of magnitudes smaller in size than those measured on Pioneer 10/11. Between 1 and 3.3 AU these experiments detected a decrease of the dust abundance proportional to $r^{(-1.5)}$ (Humes et al., 1974; Hanner et al., 1976).

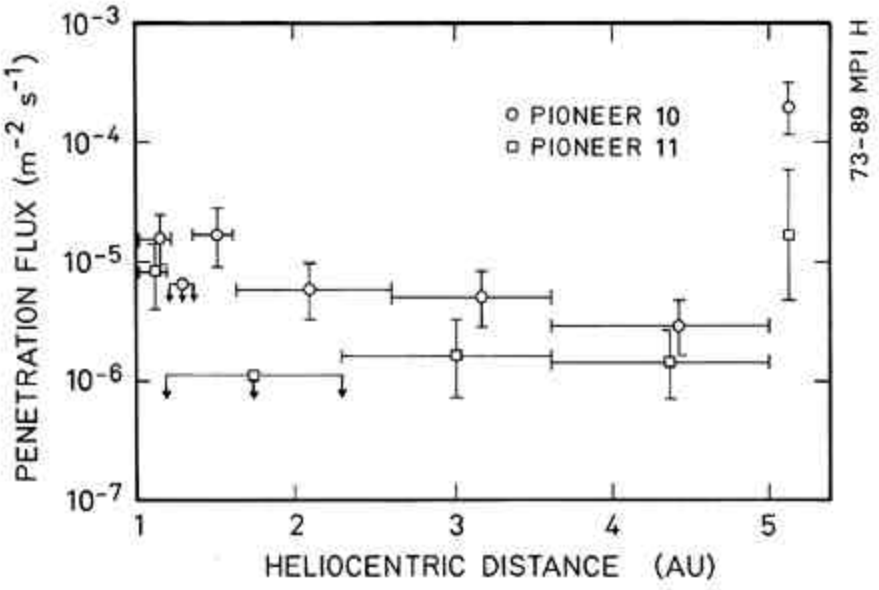

Fig. 1. Dust particle fluxes between Earth and Jupiter measured by the Pioneer 10 and 11 penetration experiments (Channel 0; Humes, 1980). The walls of the penetration cells were 25 µm and 50 µm thick stainless steel for Pioneer 10 and 11, respectively. The fluxes shown at Jupiter correspond to the average flux recorded within 50 planetary radii; the near-Jupiter peak fluxes is about an order of magnitude higher.

Within the asteroidal belt, the Pioneer 10/ 11 dust experiments (Figure 1) did not find any increase of the dust abundances as had previously been expected by some investigators. The conclusion of the experimentalists (Humes et al., 1974) was that no dust is produced in the asteroid belt. A significant increase, however, of the particles in the sensitivity range of these experiments (> 20 and 40 µm diameter) cannot necessarily be expected since the dust particles are spiraling towards the Sun and thus leaving the asteroid belt. Observation of asteroidal dust bands by the infrared satellite IRAS (Hauser et al., 1984) confirm that the asteroid belt is a significant source of dust in the solar system. Measurements of the dust population between 0.1 and 1 AU show that most of the mass of the dust grains in the inner solar system are of cometary origin (Grun et al., 1985b). At 1 AU, however, the study of lunar microcraters clearly shows that 2/3 of the projectiles which have produced the lunar micro-craters by high velocity impacts are of densities between 3 and 8 g cm^{-3} and only 1/3 of the projectiles are of low densities (< 1 g cm^{-3}). The higher density particles are most likely of asteroidal origin (Nagel et al., 1975, 1976a,b; Fechtig et al., 1975; Brownlee et al., 1973; Fechtig, 1989).

The two dust experiments on Pioneers 10/11 observed particles larger than approximately 20 µm in diameter in the outer solar system (Humes et al., 1974; Hanner et al., 1976). The most surprising result was that the photometer did not record any scattered sunlight beyond the asteroidal belt (Hanner et al., 1976) while the penetration experiment recorded dust grains at up to about 20 AU distance from the Sun at almost constant impact rate on highly eccentric orbits (Humes, 1980). Within the asteroid belt and inward to 1 AU presumably 2/3 of the dust grains are of asteroidal origin and hence recorded by both experiments in agreement with the results from lunar microcrater studies. The situation outside the asteroid belt, however, may be explained in such a way that the registered dust grains which are on high inclination orbits (Humes, 1980) are most likely of cometary origin. From the Halley investigations it is known that cometary grains have low albedos (Keller et al., 1986). With the Pioneer photometer it was not possible to distinguish the scattered sunlight of these particles from the integrated starlight background. Therefore, an explanation for the dust population outside the asteroid belt is that these dust grains are comparatively young cometary dust grains of extremely low albedos on 'cometary' orbits. For further information see Fechtig (1989).

Dust grains in interplanetary space are expected to have rather varied, and often quite complicated, dynamical histories. They will be emitted under gas pressure from comets or ejected as collisional debris from asteroids. Radiation pressure will reduce the solar gravitational force, and the orbits of the particles will spiral in towards the Sun under Poynting-Robertson and solar wind drag; these latter forces differ from particle to particle and depend on the cross-section-to-mass ratio of each individual grain. Mutual collisions between meteoroids will destroy some particles and create others from the collision fragments. Finally, the gravitational forces of the planets can have strong effects on the orbital evolutionary paths of dust grains on low inclination orbits. Numerical modeling by Jackson and Zook (1989) shows that the inner planets, and especially the Earth, are expected to trap dust grains of larger than 10 µm radius into orbits that are in orbital period resonance with the planet. They predict, in particular, that there is a heliocentric ring of dust near 1 AU that is due to dust grains trapped into exterior resonances with the

Earth. The Galileo dust detector should be suited to confirm the existence, and explore the extent of this hypothetical ring if it is a significant feature of the interplanetary dust complex.

2.2. JOVIAN DUST ENVIRONMENT

Within the Jovian system dust plays a major role in several ways. The strong gravitational field of Jupiter locally increases the interplanetary dust flux considerably. Io's volcanic activity is most likely the source for tiny particles in the Jovian magnetosphere. The many Jovian satellites are potential dust sources for ejecta particles, which are produced by meteoroid impacts. The smaller the satellites, the more effective they are as sources, because ejecta particles can more easily escape from those smaller satellites. Finally the strong Jovian magnetosphere is a potential production source for fine dust by electrostatic fragmentation of larger bodies.

The first and so far only recordings of dust in the Jovian system were obtained by the meteoroid penetration detectors on board the Pioneer 10 and 11 spacecraft. Pioneer 10 registered 11 impacts of dust particles with masses $m >= 2 \times 10^{-12}$ kg and Pioneer 11 registered 2 dust particles with masses $m >= 2 \times 10^{-11}$ kg (Humes, 1976). The corresponding peak dust flux is 2 to 3 orders of magnitudes higher than the flux in the neighboring interplanetary space.

In the neighborhood of Jupiter one has to expect the above-mentioned sources for dust. The following sections discuss these sources closer.

Gravitational focusing of interplanetary meteoroids is expected due to velocity increase within the gravitational field of Jupiter. According to Öpik (1951) the spatial flux F(R) at a distance R from a planet is given by

$$F(R) = N_0 u \left\{ 1 + \frac{v_e^2(R)}{u^2} \right\} \qquad (1)$$

with N_0 is the spatial density of dust particles in interplanetary space; $v_e(R)$, escape speed from planet at distance R; u, unaccelerated speed of meteoroids relative to the planet.

Compared to the situation near the Earth where the HEOS-2 dust experiment (Hoffmann et al., 1975) measured a gravitational increase of roughly a factor 2 one could expect an increase by a factor of 10 to 20 at Jupiter.

The Voyager spacecrafts discovered a tenuous ring around Jupiter between 1.72 and 1.81 R_J (R_J is the Jovian radius) (Owen et al., 1979; Jewitt and Danielson, 1981). Showalter et al. (1985, 1987) confirm this result and report a toroidal halo at the ring's inner edge extending inwards roughly half way to the cloud tops with a vertical thickness of about 10^4 km. For further details of the ring and its halo see Burns et al. (1984) and Showalter et al. (1987). Since the small ring particles interact with the magnetospheric plasma (Grun

et al., 1984), they have a limited lifetime of approximately 10^3 years. They are also transported out of the ring by plasma drag on a similar time scale. Because of these destruction and dispersion mechanisms, dust particles in the visible ring have to be replenished on time scales of 10^3 years. As sources for micron-sized dust particles Morfill et al. (1980b) and Burns et al. (1980) proposed the numerous large parent bodies residing within the bright ring. Small ring particles are produced by impact erosion of these large bodies. The projectiles stem from the volcanoes on Io (Morfill et al., 1980b) or are interplanetary micrometeoroids (Burns et al., 1980). A 'gossamer' ring has been discovered in the Voyager images (Showalter et al., 1985) outward of the bright ring up to a distance of ~ 3 R_J. It is quite possible that this tenuous ring extends all the way through the Jovian system.

The dust experiment on HEOS-2 (Hoffmann et al., 1975) investigated the dust population around the Earth between 5000 and 240000 km altitudes. Apart from the 'interplanetary' dust population, the experiment recorded a near-Earth increase of the dust flux. Parts of this increase - the so-called 'groups' - have been associated with lunar ejecta produced by meteoroid impacts on the surface of the Moon (Fechtig et al., 1979). Although considerable doubts have been raised as to whether or not the Moon can lose material, Zook et al. (1984) have experimentally shown that oblique impact on the Moon produces large quantities of ejecta at velocities well above the lunar escape velocities.

Jupiter with its numerous satellites - many of them smaller than the Moon - may produce considerable numbers of dust particles which contribute to the several orders of magnitude increase in dust population recorded by the Pioneer 10/11 dust experiments.

Dust particles in interplanetary space or within a planetary magnetosphere carry electrical charges. There are two competing mechanisms which charge-up particulates: photoemission of electrons by absorption of solar ultraviolet radiation and capture of impinging electrons from the ambient plasma. In interplanetary space the photoeffect generally dominates and yields a surface potential U ~ +3 to +6 V (Rhee, 1967; Wyatt, 1969). This charge has some effects on the dynamics of the interplanetary dust cloud (Morfill et al., 1986). In regions of planetary magnetosphere where the plasma density is sufficiently high dust particles are charged-up negatively to a potential which corresponds to the electron energy E_e (cf. Grun et al., 1984):

$$U \sim - \frac{E_e}{e} \qquad (2)$$

where e is the electronic charge (1.6×10^{-19} C). The charge Q on a spherical particle is then given by

$$Q = 4 \pi \varepsilon_0 U s, \qquad (3)$$

with permittivity $\epsilon_0 = 8.859 \times 10^{-12}$ C/Vm and grain radius s. Figure 2 shows dust charges and the Galileo dust detector's range of measurement.

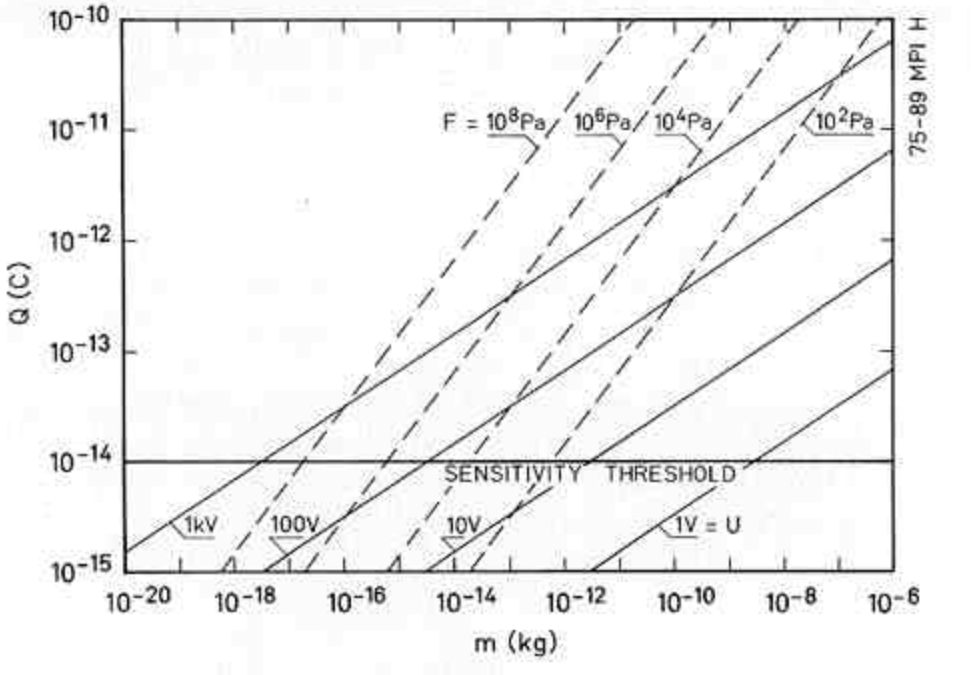

Fig. 2. Charges Q on dust particles as a function of their surface potential U (solid lines). In interplanetary space the surface potential is typically several volts positive, whereas in planetary magnetospheres it may reach a few kV negative. A particle density of rho = 1 g cm^{-3} is assumed. If the electrostatic stress $F = \epsilon_0 U/s$ (broken lines) exceeds the tensile strength of the material, the dust particle will be disrupted. Typical tensile strengths are 10^3 Pa for fluffy aggregates, 10^5-10^7 Pa for ice, and 10^6-10^3 Pa for silicates, respectively.

The HEOS-2 dust experiment recorded so-called 'dust swarms' which have been interpreted as fragmentation products due to electrostatic disruption of solids within the Earth's auroral zones (Fechtig et al., 1979). Figure 2 shows the limiting tensile strengths of the electrostatic disruption process. If such processes occur already within the Earth's magnetosphere one has to expect a much stronger effect within the Jovian magnetosphere. Depending on the location one might expect temporal and local increases up to 5 orders of magnitudes.

3. Instrument Description

3.1. EXPERIMENTAL APPROACH

The Galileo Dust Detector System (DDS) detects individual particles impacting on the sensor and measures their mass, impact speed, electric charge, and determines the impact direction. The instrument consists of an impact ionization detector and the appropriate

electronics. The impact ionization detector is similar to the HEOS-2 cosmic dust experiment, which was in Earth orbit from 1972 to 1974. The modifications to the previous experiment are (1) an increase in the sensitive area from ~ 0.01 m^2 to 0.10 m^2, (2) the addition of a measurement channel for the electrical charge of dust particles, and (3) the installation of an electron multiplier in order to obtain an additional, independent signal of dust particle impacts.

The basic sensor is shown in Figure 3. Positively or negatively charged particles entering the sensor are first detected via the charge which they induce to the charge grid while flying between the entrance and shield grids. The grids adjacent to the charge pick-up grid are kept at the same potential in order to minimize the susceptibility of the charge measurement to mechanical noise. All dust particles - charged or uncharged - are detected by the ionization they produce during the impact on the hemispherical impact sensor. After separation by an electric field, the ions and electrons of the plasma are accumulated by charge sensitive amplifiers (CSA), thus delivering two coincident pulses of opposite polarity. The rise times of the pulses, which are independent of the particle mass, decrease with increasing particle speed. From both the pulse heights and rise times, the mass and impact speed of the dust particle are derived by using empirical correlations between these four quantities. The thresholds and the dynamic ranges of the different measurements are given in Table III.

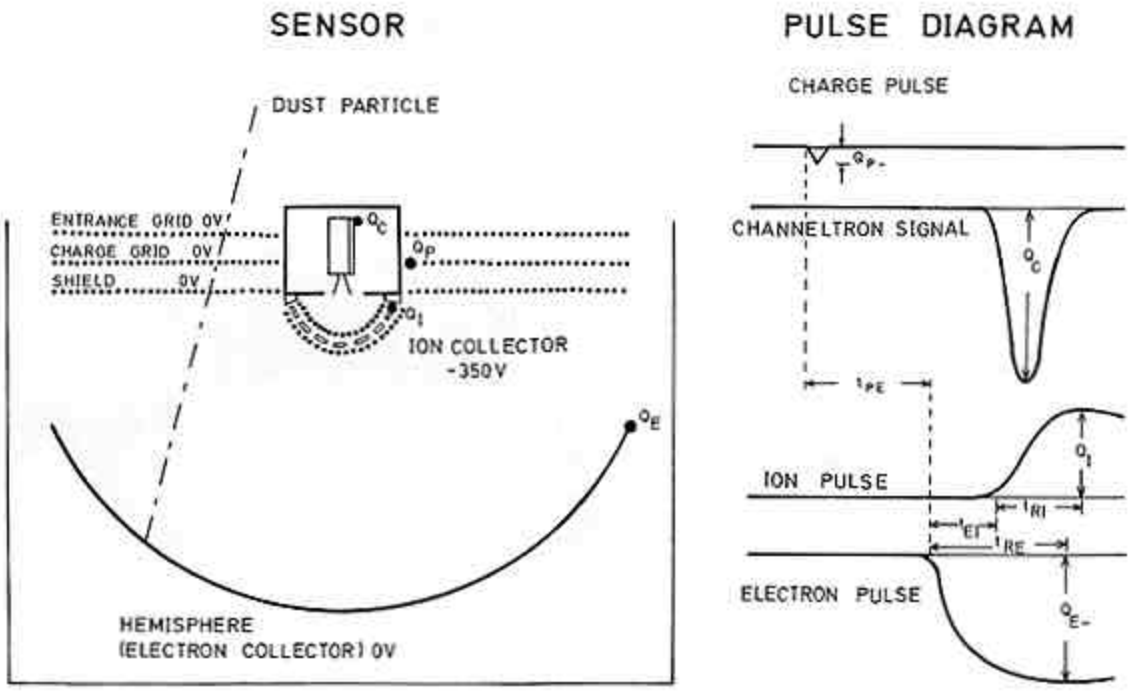

Fig. 3. Sensor configuration (schematic) and measured signals upon impact of a negatively charged dust particle.

A third independent signal originates from part of the positive impact charge which is detected and amplified (approx. x 100) by an electron multiplier (channeltron). This signal serves as a control for the identification of dust impacts. The multiplier has a low dark current at the required amplification. Channeltron gain loss will be compensated by changes in the channeltron voltage, which will be effected by telecommand. An impact event just exceeding the detection threshold of the instrument (corresponding to 10^{-14} C) will result in an output signal from the channeltron of ~ 10^{-12} C, On one hand, noise events (microphonics or electromagnetic interferences) that exceed the CSA threshold will produce smaller output signal at the channeltron. On the other hand energetic particles which may stimulate the channeltron are less effective at the channels which measure the charge by means of CSAs. Therefore one has an umambiguous method of distinguishing noise events from impact events by measuring the channeltron output signal and deriving coincidence signals between both CSAs and the channeltron. This information is used by the on-board processor to give higher priority to the transmission of data from impact events than to those from noise events (see below).

From Table III it can be seen, that the amplitude of the positive and negative charge pulses, the channeltron signal and the corresponding rise times are redundant measures of mass and impact speed of the dust particle. This redundancy gives a further check on the identification of an impact event and increases the accuracy of the measurement considerably. In order to further increase the reliability of impact identification coincidences between the different signals are derived and evaluated in an event classification scheme. The instrument and its operation are designed to reliably suppress noise and allow detection of as few as one impact event per month, the charge of which is close to the detection threshold. This is about a factor of 10 below the lowest expected dust particle flux.

TABLE III

Signals measured by the Galileo Dust Detector upon impact of a dust particle onto the sensor and related particle parameters

Signal designation	Measured quantity	Range	Accuracy (number of logarithmic steps)	Related particle parameters
Q_E	Negative charge generated upon impact (electrons)	10^{-14} - 10^{-8} C	48	Mass, speed
Q_I	Positive charge generated upon impact (ions)	10^{-14} - 10^{-8} C	48	Mass, speed

Q_C	Positive charge generated upon impact (partially)	10^{-13} - 10^{-9} C (channeltron output)	32	Impact identfication (mass, speed)
Q_P	Induced charge positive Induced charge negative	10^{-14} - 10^{-12} C 10^{-14} - 10^{-10} C	16 32	Electric charge
t_E	Rise time of negative charge	10-100 µs	16	Speed
t_I	Rise time of positive charge	10-100 µs	16	Speed
t_{EI}	Time difference negative positive charge signals	1-50 µs	16	Impact identification
t_{PE}	Time difference induced negative charge signals	1-400 µs	32	Speed

3.2. ANGULAR SENSITIVITY AND SENSOR POINTING

The geometric detection probability is defined by the sensitivity of the detector for particles impinging from different directions in an isotropic flux of particles. Directions are determined by an angle theta to the sensor axis.

The angular sensitivity was calculated by a computer simulation program that 'fired' a particle beam onto the sensor from different directions. The cross-section A of the beam, which hit the target, was calculated. This is predominantly a cosine function; for larger incidence angles theta it is modified by the shielding of the detector's side walls. The maximum area (0.10 m^2), of course, is found for theta = 0 (Figure 4). Because of the axial symmetry of the detector, the solid angle interval is (d OMEGA = 2 pi sin theta d theta). The relative sensitivity I(theta) is therefore given by

$$I(\theta)\, d\Omega = \frac{A(\theta)}{A(\theta = 0)}\, 2\pi \sin\theta\, d\theta \qquad (4)$$

Integration of this function leads to the effective solid angle interval covered by the detector, which is 1.45 sr (cf. Goller and Grun, 1989).

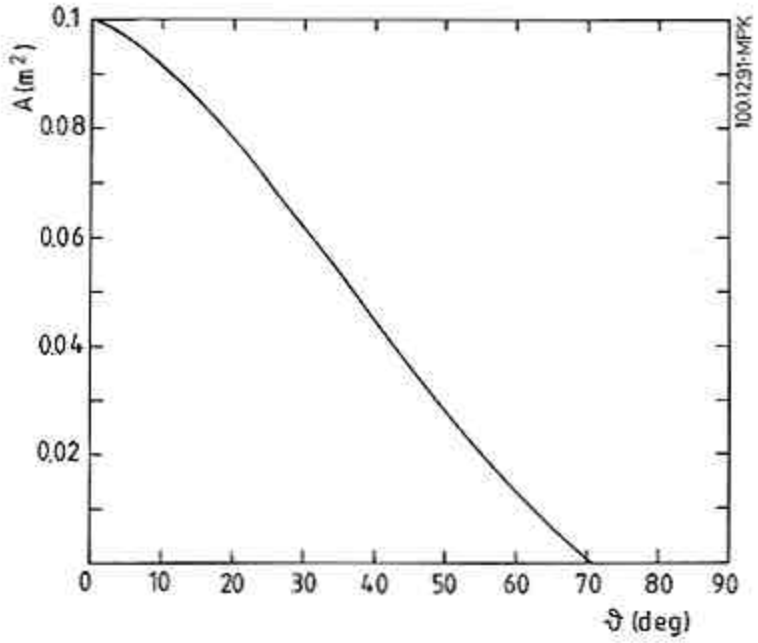

Fig. 4. Angular sensitivity. The sensitive area A is shown as a function of angle theta with respect to the sensor axis. In an isotropic flux, 50% of all particles will impact the sensor at theta < 32°.

The distribution of the impact angles onto the target was determined in a similar way. Impact angles were measured between particle direction and the normal of the target at the impact point. As the target was curved they were generally different from the incidence angles theta (measured to the sensor axis). The average impact angle was 36°. As the calibration differed slightly for different impact angles their distribution was used for finding the proper average calibration curve.

In addition the distribution of flight paths inside the detector was determined. Depending on incidence angle and point of impact at the target, the particles had different flight paths. This part of the calculation was done to determine the average pathlength and its deviations, to find a conversion from time of flight (t_{PE}) to particle speed. The average flight path of a particle in the detector was 20 cm +/- 5 cm. The uncertainty given refers to 68% of all trajectories.

The sensor is mounted to the science boom on the spinning section of the spacecraft. For reasons of the experiment's simplicity and reliability, as well as for keeping the weight low, the pointing direction of DDS was fixed at a single angle with respect to the spacecraft spin axis. The chosen angle of 55°. with respect to the positive spin axis (z-axis of the spacecraft) appeared to provide optimal conditions for detecting, and then analyzing a variety of known and potential cosmic dust families and their trajectories, especially in the Jovian system.

3.3. TECHNICAL DESCRIPTION

The whole instrument comprises a sensor with channeltron and pre-amplifiers, signal conditioning, and spacecraft interface electronics. The latter two are separated from the sensor and pre-amplifiers, and included in the electronics box (Figure 5).

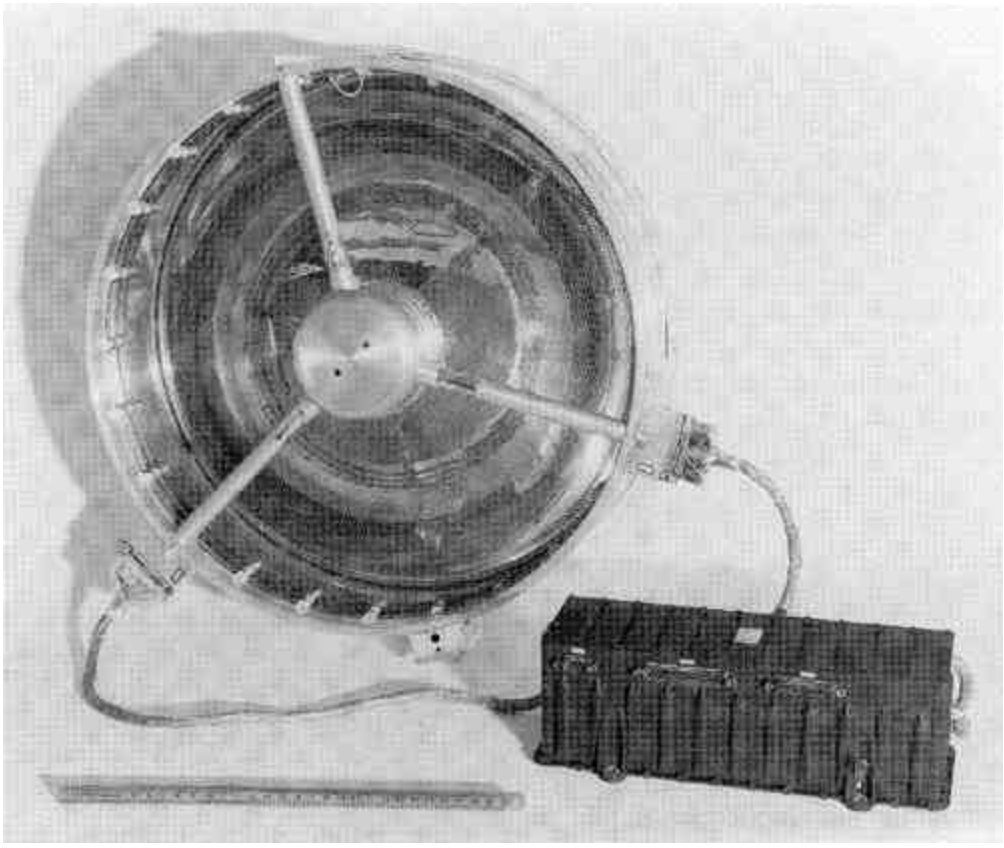

Fig. 5. Sensor and electronics box of the Galileo Dust Detector.

The sensor consists of a grid system for the measurement of the particle charge, an electrically grounded target (hemisphere) and a negatively biased ion collector (Figure 3). A charged dust particle entering the sensor will induce a charge to the charge grid, which is connected to a charge sensitive amplifier. The output voltage of this amplifier rises until the particle passes this grid, and falls off to zero when it reaches the shield grid. The peak value (Q_P) is stored for a maximum of 600 µs and is only processed if an impact is detected by the impact ionization detector within this time. A dust particle hitting the hemispherical target produces electrons and ions, which are separated by the electric field between hemisphere and ion collector into negative charges (electrons and negative ions) and positive ions. The negative charges are collected at the hemisphere and measured by a charge sensitive amplifier (Q_E). Positive ions are collected and measured at the negatively biased ion collector with a charge sensitive amplifier (Q_I). Some of the ions penetrate the ion collector, which is partly transparent (total transmission approximately 40%), are further accelerated, and hit the entrance cone of an electron multiplier (channeltron). Secondary electrons are produced, amplified, and measured by a charge sensitive amplifier (Q_C). Other quantities measured, are the rise times (t_I, t_E) of both the positive and negative charge pulses (Q_I and Q_E) The measurement of the time delay (t_{EI})

between electron pulse and ion pulse serves as a means for distinguishing impact events from noise. Impact events have time delays of 2-50 °s, while mechanical noise has a time delay of milliseconds. These signal amplitudes and times of a single recorded event are digitized and stored in an Experiment Data Frame (EDF).

A measurement cycle is initiated if either the negative charge QE on the hemispherical target, or the positive charge on the ion-collector Q_I or Q_C exceeds a threshold. Since the hemisphere has a large area which is directly exposed to interplanetary plasma and high-energy radiation, we expect that this may cause some interferences for the Q_E measurement. To avoid these interferences during high activity times, it is possible to switch by command to a mode in which a measurement cycle is initiated if only the charge on the ion collector Q_I (small area and not directly exposed) or channeltron signal Q_C exceeds the threshold. If more than one event occur within the transmission time of one EDF, then these events are counted by several amplitude-dependent counters. The dead-time caused by the measurement cycle is 5 ms.

Figure 6 shows a block diagram of the instrument. The signals from the sensor are conditioned and analysed. The microprocessor coordinates the experiment measurement cycle, collects the buffered measurement data and processes the data according to a program stored in the memory.

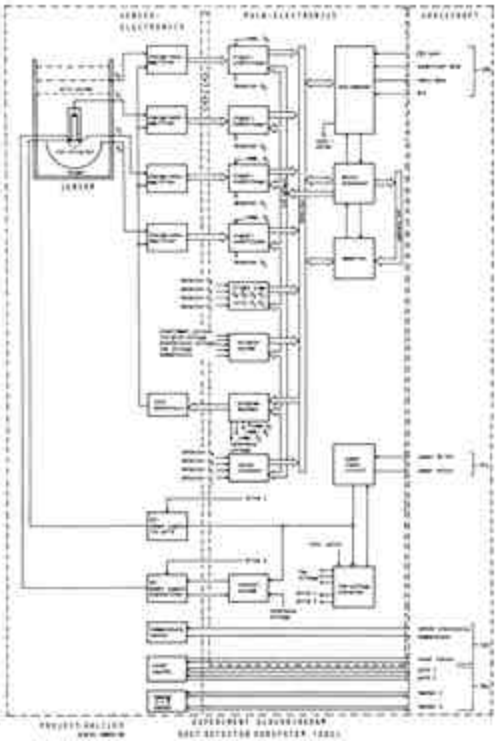

Fig. 6. Functional block diagram of the Galileo Dust Detector.

For a larger view: Fig 6. (334k)

Each event recorded by the instrument is classified according to its ion signal amplitude into 6 amplitude intervals of about one decade width. In addition each event is categorized by one out of four event classes. Class 0 are all events (noise events and some unusual impact events - e.g., hits of the sensor's internal structure) which are not categorized in a higher class. For class 1 through class 3 events the measured parameters and their relation to each other are increasingly restricted, so that class 2 represents 'potential' and class 3 represents 'probable' dust impact events. Data from events of all classes are buffered in the A-range of the instrument memory. This range contains complete data sets from 6 events of different ion signal amplitudes. In addition up to eight class 3 events are stored in the E-range of the instrument memory. This classification scheme is initially optimized to laboratory noise conditions but it is also adaptable to the in-flight noise situation by changing the classification parameters (set points) or by adjusting the onboard classification program by commands. Detailed information on noise is mandatory in order to evaluate the reliability of impact detection as well as to determine the effect on the dead-time of the instrument.

Each event is counted in one out of 24 counters according to its ion amplitude and event class. The scheme of the 24 accumulators (ACs) is shown in Table IV. Fourteen EDFs (each containing the full information on a single event and the corresponding accumulator contents) are stored in the memory and are shifted sequentially through the bus adapter to the spacecraft. The exchange of data with the spacecraft and instrument modes are controlled by the microprocessor. An internal test generator stimulates and calibrates the electronics periodically or by command and generates 'test pulse-data'.

TABLE IV

Scheme of DDS accumulators

Class number		C0	C1	C2	C3
Amplitude range	A1	AC01	AC11	AC21	AC31
	A2	AC02	AC12	AC22	AC32
	A3	AC03	AC13	AC23	AC33
	A4	AC04	AC14	AC24	AC34
	A5	AC05	AC15	AC25	AC35
	A6	AC06	AC16	AC26	AC36

3.4. INSTRUMENT DATA

In this paragraph DDS data, its data transmission modes and its initial on-ground processing steps are described. All information on events (dust impacts or noise) recorded by the instrument is contained in data packages of 16 bytes (1 byte = 8 bits) of

science data which are supplemented by 10 bytes of engineering housekeeping data (Table V). DDS data are generally transmitted within the Low Rate Science (LRS) mode.

One EDF consists of 26 bytes and is read out from the instrument to the spacecraft within 13 Low Rate Science frames (LRS) and with 2 bytes of data contained in each LRS. Apart from science data there are also other types of DDS data which are transmitted (cf. Table V), depending on the mode selected:

- Mode 1 is the science collection mode, the first 16 bytes of data contain science data and the next 10 bytes housekeeping information,
- Mode 2 is the memory read-out mode, in this mode the first 2 bytes contain the 16 bits starting address of the memory readout. The next 13 bytes of data contain readout data from any part of the instrument memory (ROM or RAM, depending on the starting address). The 10 bytes housekeeping data and status information are the same as describe in mode 1, and
- Mode 3 is the instrument set point mode; two packets of DDS data will contain the actual set point data information.

In addition to mode 2, DDS has another capability to read out the memory data by using the direct memory transfer to the spacecraft. In this case it is possible to read out the memory data in packets of 32 bytes.

TABLE V

Data of the Galileo Dust Detector. One Experiment Data Frame (EDF) contains 208 bits: 128 bits of science data recorded for one event and 80 bits of housekeeping data. In special modes the memory content or instrument set points are read-out.

Name	Bits	Description
		Science data
CA	5	Amplitude of channeltron signal Q_C.
CCP	2	Channeltron (Q_C) threshold setting
CL0	8	Class 0 counter, 6 amplitude ranges
CL1	8	Class 1 counter, 6 amplitude ranges
CL2	8	Class 2 counter, 6 amplitude ranges
CL3	8	Class 3 counter, 6 amplitude ranges
CLN	2	Class number of transmitted event
CN	4	Channeltron noise counter, which counts all threshold exceedings. The counter is reset every 81 ms
EA	6	Amplitude of negative charge QE. measured at the target
ECP	2	Negative charge (Q_E) threshold setting

EIC	1	Coincidence between negative and positive charge signals: if both pulses exceed the thresholds in a time interval of 200 ns
EIT	4	Time tEI measured between negative and ion charge signals
EN	4	Negative charge noise counter, which counts all threshold exceedings. The counter is reset every 41 ms
ERS	3	E-range frame number
ET	4	Rise time tE of negative charge signal
EVD	3	Event definition status, indicates the actual setting for the initiation of data acquisition by one or more measuring channels (negative charge-, ion- or channeltron signal)
FN	3	Data frame number, indicator for EDF content: A-range or E-range science data, set point data 1 or 2, commanded or automatic testpulse data or memory content
IA	6	Amplitude of ion charge QI measured at the ion grid
ICC	1	Coincidence between ion and channeltron signals: if both pulses exceed the thresholds in a time interval of 20μs
ICP	2	Ion charge (Q_I) threshold setting
IN	4	Ion noise counter, which counts all threshold exceedings. The counter is reset every 81 ms
IT	4	Rise time tI of ion charge signal
PA	6	Amplitude of induced charge QP, most significant bit indicates polarity
PCP	2	Induced charge (Q_P) threshold setting
PET	5	Time difference tPE between induced and negative charge signals
PN	4	Induced charge noise counter, which counts all threshold exceedings. The counter is reset every 10 ms
SEC	8	Spacecraft sector at time of event
SES	1	Sector data status, sector data valid or not valid
THS	1	Threshold status, indicator bit for threshold settings by command or automatically by each individual noise counter
TIME	8	Spacecraft event time; short time interval: 121.33 s, 1.33 s step size; long time interval: 138 hr 32.35 min step size
TS	1	Transmit status of EDF: first time or repeated transmission

Housekeeping data

ADD-HK	2	Address counter, determines whether the transmitted byte contains the sub-commutated word PARN, CMD-ACC, or CMD-REJ

CMD-ACC	8	Command accepted, counts all commands which are identified as DDS commands
CMD-REJ	8	Command rejected, counts all unrecognized commands
CMP-S	8	Computer status, contains information about computers and memories and a 1-bit indicator for the spacecraft event time interval
CUR	8	Experiment current, range 15 to 100 mA
HVC	8	Channeltron high voltage, range 0 to 2500 V
HVI	8	Ion grid high voltage, range 0 to -512 V
PARN	8	Parity error number, counts all supervisory data parity errors
SYNC	6	Synchronization word
TEMP	8	Main electronics box temperature, range -30° to +80° C
VA +	8	Low voltage + 7.5 V, range 0 to 10 V
VA -	8	Low voltage - 7.5 V, range 0 to -10 V
VD+	8	Low voltage + 10 V, range 0 to 15 V
		Memory readout and Set Point data
MHAD	8	Memory high address
MLAD	8	Memory low address
MEMC	8	Memory content
SP1 to SP18	8	Instrument set point data, 18 words

During normal Low Rate Science data transmission one EDF is sent every 8.7 s, which corresponds to an average DDS data transmission rate of 24 bits s^{-1}. During interplanetary cruise and during orbital cruise around Jupiter one or two passes (of about 8 hr duration) of LRS data per week will be transmitted. This rate corresponds to an average DDS data rate of 1-2 bits s^{-1}. During the first phase of the mission, i.e., to Venus and back to Earth, when the high gain antenna cannot be used, DDS data are fed into the engineering data stream at an average rate of 0.01 bits s^{-1}. For this period E-range data (class 3 events) and accumulator data are transmitted with high priority.

Data received from DDS on ground will be initially evaluated according to the following scheme:

1. Probable impact events, potential impact events, and noise data are extracted from the raw data and put into separate files. Count rates of probable events (class 3 counters) are accumulated over fixed time intervals and transferred to the Common Data File, which is shared among the Fields and Particles investigators.
2. Statistical analysis of the noise data will result in a Dead-Time History File, with the help of which impact rates can be accurately determined.
3. Identification of all dust impact data and calibration of this data will result in a Physical Parameter File, which then can be used for further analysis by the DDS investigator team.

3.5. CALIBRATION

Extensive calibration tests have been performed with the Galileo Dust Detector (Goller and Grun, 1985, 1989) at the Heidelberg dust accelerator. Calibration tests were performed with iron, carbon, and silicate particles. The particles were in the speed range from 1 km s^{-1} to 70 km s^{-1} and in the mass range from 10^{-18} kg to 10^{-13} kg. In addition to the projectile material variation, we carried out calibration tests for iron particles, and varied the impact angles.

There are three possibilities to determine a particle's speed: the rise times t_I, t_E, and the ratio Q_C/Q_I. Figure 7 shows the dependency of the rise time of the ion charge signal as a function of the impact speed. If we use all three measurements the speed can be determined with an accuracy of a factor of 1.6. Using only one measurement the accuracy is about a factor 2.

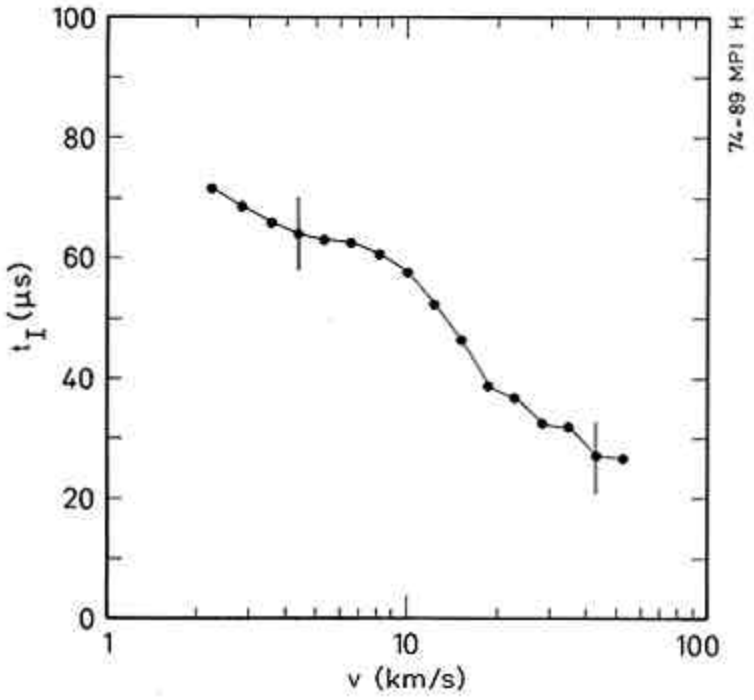

Fig. 7. Rise time tI of the ion charge signal as a function of the impact speed v for iron particles (from Goller, 1988).

When the particle speed is known, the mass can be determined from the charge yields Q_I/m and Q_E/m. If the speed is known within a factor of 1.6 and both yields are used for mass determinations the value can be measured with an uncertainty of a factor of 6. The main part of this error is caused by the limited accuracy of the speed measurement.

From the charge yields the sensitivity of the sensor can be calculated. The negative charge pulses have higher yields than the positive pulses. This fact is mainly caused by

some positive ions leaving the detector after impact. Thus they are not collected by the ion collector.

The speed-dependent measurable mass range is shown in Figure 8. Under flight conditions, especially if the noise level is high, the electronic detection threshold can be set to a higher value. In this case the sensitivity will be reduced. Since the charge sensitive amplifiers cover a range of six orders of magnitude, the upper limit for particle measurement is also indicated (saturation range). For larger particles the detector operates as a threshold detector. The calibration covered a speed interval ranging from about 2 km s^{-1} to 70 km s^{-1} (see Figure 8).

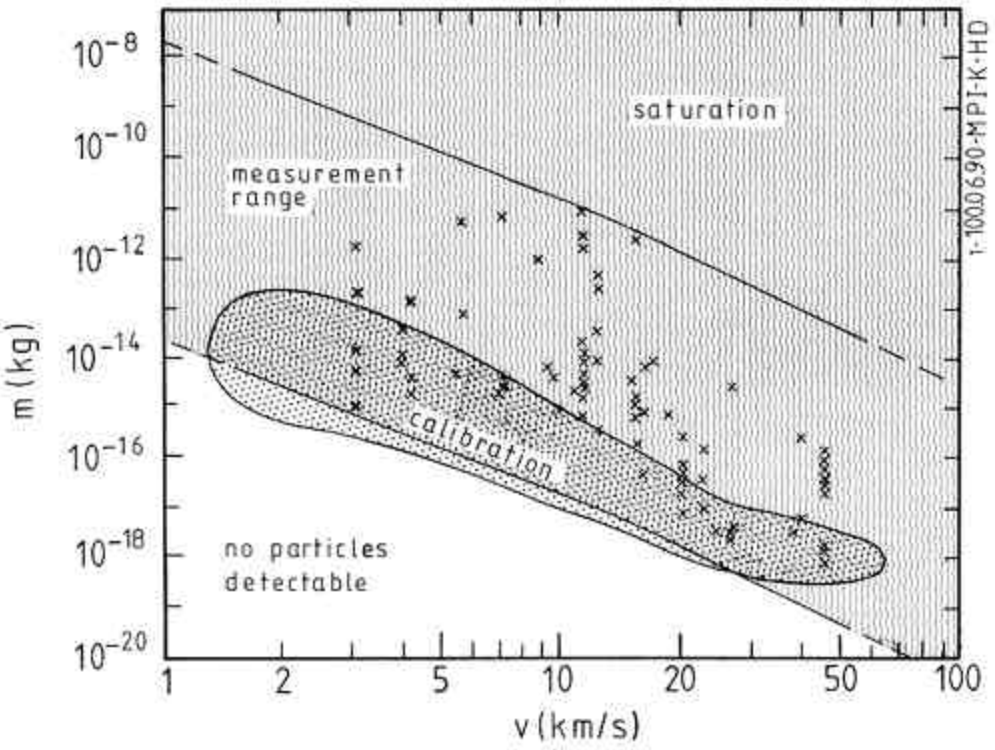

Fig. 8. Dust particle masses and speeds which can be measured by the Galileo Dust Detector. In the region marked 'saturation' the instrument operates as a threshold detector. The mass and speed range is indicated, in which the instrument was calibrated with silicate, carbon, and iron particles. Shown are also mass and speed values for the 81 discrete impacts detected in all but the lowest amplitude/class ranges until May 18, 1990. The accuracies are factors 2 and 10 for speed and mass values, respectively.

3.6. MEASUREMENT RANGES AND PAYLOAD PARAMETERS

The impact rate will be measured from 3 x 10^{-7} s^{-1} to 10^{2} s^{-1} in order to cover both the impact rates expected in interplanetary space and during times of high activity (e.g., in the Jovian magnetosphere).

The measurable particle mass ranges from 10^{-19} kg < m < 10^{-13} kg at 40 km s^{-1} to 10^{-16} kg < m < 10^{-10} kg at 5 km s^{-1} impact speed. The detectable impact speed is v >= 1 km s^{-1}. The particles, electric charges are measured from 10^{-14} C to 10^{-10} C for negative charges and 10^{-14} C to 10^{-12} C for positive charges. The maximum angle of incidence for dust particles with respect to the sensor axis will be 70°.

The volumetric envelope of the sensor is cylindrical: 442 mm in diameter and 301 mm long (without cover). The electronics box has a volume of 283 x 100 x 100 mm^3. The total weight of the instrument is 4.2 kg and its power consumption is 2.4 W plus up to 3.0 W for heaters. The average data transmission rate is 24 bit s^{-1} in spacecraft tracking mode. The operating temperature limits are -20° C to +40° C.

4. Initial Performance

The following report provides a summary of the performance of the Galileo DDS instrument as observed during the 4-day science check-out period from December 27 to 30, 1989 (during this period about 8 hours per day of LRS data was available) and includes data from 26 instruments memory read-outs until May 18, 1990.

On December 27 the DDS cover was successfully deployed as indicated by the microswitch status change and the sensor temperature decrease which was as expected. On December 28 DDS was switched on for the first time. All functions were successfully checked-out. When the instrument was switched to the measuring mode, low amplitude noise on three (EA, CA, and PA) out of four charge measuring channel was detected. Such noise has never been observed during ground tests. An internal or external noise source could not be identified during the 4-day check-out and subsequent periods. By help of real-time commanding DDS was brought into a state where it was immune against the types of noise encountered initially.

Around Venus encounter high noise rate was detected also at the ion channel (IA). This noise seems to have caused increased dead-time starting at least February 8, 1990. By commanding (on February 16, 1990) the detection threshold was increased to step one (IA >= 3) and the noise rate was reduced to very low values thereafter.

Noise events have been observed only in amplitude/class ranges AC01, AC11, and AC02 (cf. Table IV), although some impacts of these types have been identified as well in the discrete data. Only impact events were recorded by all other accumulators. Therefore, the contents of AC01. AC11, and AC02 are used for determining the maximum noise rate, whereas all other accumulators are added-up in order to determine the impact rate.

A summary of the discretely recorded dust impacts is displayed in Figure 9. The positions of Galileo, Venus, and Earth for May 18, 1990 are indicated. Recorded dust impacts are overlaid on Galileo's orbit. The impact direct direction distribution shows the predominance of impacts from the apex direction, an effect which was observed also by previous dust detectors (Berg and Grun, 1973; Grun et al., 1985a; Hoffmann et al., 1975). Gaps apparent in the distribution of impacts, are due to two about 4-weeks long gaps in

the data transmission during which an overflow in the internal memory assigned for discrete impact data occurred.

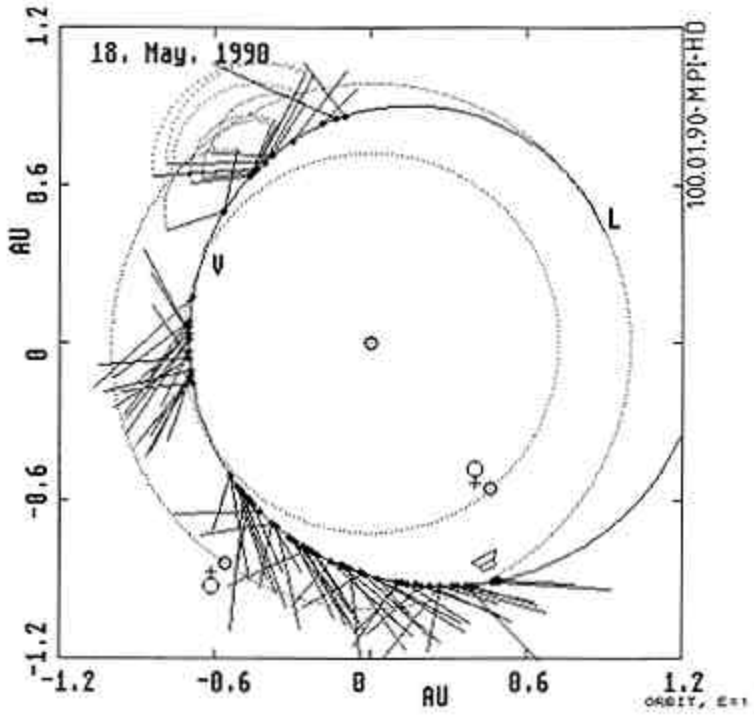

Fig. 9. Orbit of the Galileo spacecraft and impacts recorded until May 18, 1990. The positions for this date of Galileo, Venus and Earth are indicated. Dust impacts (dots) are overlaid on Galileo's orbit. Ecliptic projections of the sensor pointings are indicated by attached bars. No pointing information was obtained for impacts Nos. 7 to 13, here the full range of sensor pointings is shown. The length of the bars represents the magnitude of the impact charge (IA).

Preliminary particle parameters have been calculated for the recorded discrete impacts. The physical parameters are based on IA-, EA-, IT-, and ET-data only and on calibration with iron particles. CA-information has not yet been used because we do not have accurately determined the channeltron amplification yet. An effect of the low channeltron voltage is the increased amplitude range in which class number 0 events occur. Therefore, small events (IA <= 15) are not complete.

During the first 141 days of DDS operation, the dust experiment has detected and accumulated at least 168 impacts in all but the lowest amplitude/class ranges. Eighty-one of these dust particles have been recorded by measuring the individual masses and speeds relative to the sensor. Preliminary impact speeds are determined so far only in the range 3 to 50 km s^{-1}. Figure 8 shows the masses and speeds of the recorded dust particles in relation to the measurement range. The accuracy of the speed is about a factor two and that of the masses is about an order of magnitude. In the lower 1/3 of the measurement range (about 2 orders of magnitude in mass) the true particle distribution is significantly

under-represented because of instrumental limitations. No electric charge carried by dust particles has been identified so far.

From the accumulated impact events it was possible to calculate total fluxes. For comparison, three flux values are given: (a) flux phi between 0.875 AU (DDS switch-on) and perihelion (0.698 AU), (b) between perihelion and 0.875 AU, and (c) between 0.875 AU and 1.035 AU. These fluxes are (referring to 1.45 sr effective solid angle):

(a) phi = 8.5 x 10^{-5} m^{-2} s^{-1} between 0.875 AU and perihelion.
(b) phi = 2.1 x 10^{-4} m^{-2} s^{-1} between perihelion and 0.875 AU.
(c) phi = 1.3 x 10^{-4} m^{-2} s^{-1} between 0.875 and 1.035 AU.

It is remarkable that the inbound and outbound fluxes between 0.875 AU and perihelion are almost a factor 2.5 different from each other. This has to do with the orientation of the viewing cone of the dust sensor relative to the orbit of the spacecraft. In the outbound section the fluxes are comparatively higher because the spacecraft motion is outward towards the hemisphere the sensor is facing (cf. Figure 9). The decrease of the flux around 1 AU in the third section in comparison with the flux close to the Sun is due to the decrease of the dust population with increasing distance from the Sun (in qualitative agreement with relevant from the Helios dust experiment, Grun et al., 1985a).

As shown in Figure 8 the recorded dust grains are generally between 10^{-18} kg and 10^{-11} kg. However, the mass threshold depends on the relative speed of the dust particles and the dust sensor. 10^{-18} kg is correct at a speed of approximately 30 km s^{-1}, but for 3 km s^{-1} the smallest mass observed is only 10^{-15} kg. The mean mass threshold of the reported flux is about 10^{-17} kg (about 0.3 µm diameter) and corresponds to a speed of roughly 20 km s^{-1} These flux values are comparable to the in-ecliptic flux observed at 1 AU (1.1 x 10^{-4} m^{-2} s^{-1} for m >= 10^{-17} kg and 1.4 sr: Grun et al., 1985b). Conclusions concerning the orbit distribution of the interplanetary dust particles have to wait for further analysis.

Acknowledgements

The development, implementation, and testing of this instrument and its data processing system was only made possible by the efforts of a great number of individuals from various departments of the Max-Planck-Institut fur Kernphysik and from outside institutions and companies. The authors are especially indebted to G. Baust. H. Geldner, J. R. Goller, R. Hofacker, O. Kress, G. Linkert, G. Matt, C. Nehls, D. Roemer, H. Sallmutter, G. Schafer, W. Schneider, N. Siddique, O. Titze, and A. Zahlten for their personal involvement during that campaign. Important contributions came from P. Gammelin, F. Eckl, and D. Semder of ARGE PEES, W. Fischer and G. Pahl of Walter Fischer Geratebau, and A. Kaiser of Ingenieurburo Kaiser. Careful attention and effective coordination and support has been provided by W. Kempe of DLR and by M. Agabra, C. J. Coppock, W. Fawcett, G. McSmith, C. Polanskey, and the Galileo Instrument Team of JPL. We are grateful for the support received from the Galileo project scientist T. V. Johnson. We thank E. Schwarzenbacher for the careful preparation of this manuscript.

This work has been supported by the Bundesminister fur Forschung and Technologie, under the grands 01QJ087-WRF7701 and 01QJ900400.

References

Acuna, M. H. and Ness, N. F.: 1967, 'The Complex Main Magnetic Field of Jupiter', J. Geophys. Res. 81, 291 7.

Berg, O. E. and Grun, E.: 1973, in 'Evidence of Hyperbolic Cosmic Dust Particles', Space Research XIII, Akademie Verlag, Berlin, pp. 1047-1055.

Brownlee, D. E., Horz, F., Vedder, J. F., Gault, D. E., and Hartung, J. B.: 1973, 'Some Physical Parameters of Micrometeoroids', Proc. Lunar Sci. Conf 4, 3197.

Burns, J. A., Showalter, M. R., Cuzzi, J. N., and Pollack, J. B.: 1980, 'Physical Processes in Jupiter's Ring: Clues to Its Origin by Jove!', Icarus 44, 339.

Burns, J. A., Showalter, M. R., and Morfill, G. E.: 1984, in R. Greenberg and A. Brahic (eds.), 'The Ethereal Rings of Jupiter and Saturn', Planetary Rings, University of Arizona Press, Tucson, pp. 200-272.

Dietzel, H., Eichhorn, G., Fechtig, H., Gran, E., Hoffmann, H.-J., and Kissel, J.: 1973, 'The HEOS 2 and Helios Micrometeoroid Experiments', J. Phys. (E) Sci. Instr. 6, 209.

Fechtig, H.: 1989, 'Dust in the Solar System', Z. Naturforsch. 44a, 877.

Fechtig, H., Gentner, W., Hartung, J. B., Nagel, K., Neukum, G., Schneider, E., and Storzer, D.: 1975, 'Microcraters on Lunar Samples', Proc. Soviet-American Conference on Cosmochemistry, Moscow, pp. 453-472 (translation: NASA SP-370, pp. 585-603).

Fechtig, H., Grun, E., and Kissel, J.: 1978, in J. A. M. McDonnell (ed.), 'Laboratory Simulation', Cosmic Dust, Wiley and Sons, Chichester, pp. 607-669.

Fechtig, H., Grun, E., and Morfill, G.: 1979, 'Micrometeoroids within Ten Earth Radii', Planetary Space Sci. 27, 511.

Fillius, W.: 1976, in T. Gehrels (ed.), 'The Trapped Radiation Belts of Jupiter', Jupiter, University of Arizona Press, Tucson, pp. 896-927.

Friichtenicht, J.F. and Slattery, J.C.: 1963, Ionization Associated with Hyper velocity Impact, NASA Technical Note D-2091.

Goller, J. R.: 1988, 'Kalibrationsmesungen an Mikrometeoriten far die Missionen Ulysses, Galileo und Giotto', Ph.D. dissertation, University of Heidelberg, Heidelberg.

Goller, J. R. and Grun, E.: 1985, in R. H. Giese and P. Lamy (eds.), 'Calibration of the Galileo/ISPM Dust Detectors with Iron Particles', Properties and Interactions of Interplanetary Dust, D. Reidel Publ. Co., Dordrecht, Holland, pp. 113-115.

Goller, J. R. and Grun, E.: 1989, 'Calibration of the Galileo/Ulysses Dust Detectors with Different Projectile Materials and at Varying Impact Angles', Planetary Space Sci. 37, 1197.

Grun, E., Berg, O. E., and Dohnanyi, J. S.: 1973, in M. J. Rycroft and S. K. Runcorn (eds.), 'Reliability of Cosmic Dust Data from Pioneers 8 and 9', Space Research XIII, Akademie Verlag, Berlin, pp. 1057-1062.

Grun, E., Morfill, G., Schwenn, G., and Johnson, T. V.: 1980, 'A Model of the Origin of the Jovian Ring', Icarus 44, 326.

Grun, E., Fechtig, H., Giese, R. H., Kissel, J., Linkert, D., McDonnell, J. A. M., Morfill, G. E., Schwehm, G., and Zook, H. A.: 1983, in K. P. Wenzel, R. G. Marsden, and B. Battrick (eds.), 'The ISPM Dust Experiment', The International Solar Polar Mission - Its Scientific Investigations, ESA SP-1050, pp. 227-241.

Grun, E., Morfill, G. E., and Mendis, D. A.: 1984, in R. Greenberg and A. Brahic (eds.), 'Dust-Magnetosphere Interactions', Planetary Rings, University of Arizona Press, Tucson, pp. 275-332. Grun, E., Fechtig, H., and Kissel, J.: 1985a, in R. H. Giese and P. Lamy (eds.), 'Orbits of Interplanetary Dust Particles Inside I AU as Observed by Helios', Properties and Interactions of Interplanetary Dust, D. Reidel Publ. Co., Dordrecht, Holland, pp. 105-111.

Grun, E., Zook, H. A., Fechtig, H., and Giese, R. H.: 1985b, 'Collisional Balance of the Meteoritic Complex', Icarus 62, 244.

Hanner, M. S., Sparrow, J. G., Weinberg, J. L., and Beeson, D. E.: 1976, in 'Pioneer 10 Observations of Zodiacal Light Brightness Near the Ecliptic: Changes with Heliocentric Distances', Interplanetary Dust and Zodiacal Light, Lecture Notes in Physics 48, 29.

Hauser, M. G., Gillett, F. C., Low, F. J., Gautier, T. N., Beichmann, C. A., Neugebauer, G., Aumann, H. H, Band, B., Boggess, N., Emerson, J. P., Houck, J. R., Soifer, B. T., and Walker, R. G.: 1984, 'IRAS Observations of the Diffuse Infrared Background'. Astrophys. J. 278, L15.

Hoffmann, H.-J., Fechtig, H., Grun, E., and Kissel, J.: 1975, 'Temporal Fluctuation and Anistropy of the Micrometeoroid Flux in the Earth-Moon System', Planetary Space Sci. 23, 985.

Hoffmann, H.-J., Fechtig, H., Grun, E., and Kissel, J.: 1976, in B. Donn et al. (eds.), 'Particles from Comet Kohoutek Detected by the Micrometeoroid Experiment of HEOS 2', The Study of Comets, NASA SP-393, pp. 949-961.

Humes, D. H.: 1976, in T. Gehrels (ed.), 'The Jovian Meteoroid Environment', Jupiter, University of Arizona Press, Tucson, pp. 1052-1067.

Humes, D. H.: 1980, 'Results of Pioneer 10 and 11 Meteoroid Experiments: Interplanetary and Near- Saturn', J. Geophys. Res. 85, 5841.

Humes, D. H., Alvarez, J. M., O'Neal, R. L., and Kinard, W. H.: 1974, 'The Interplanetary and Near-Jupiter Meteoroid Environment', J. Geophys. Kes. 79, 3677.

Jackson, A. A. and Zook, H. A.: 1989, 'A Solar System Dust Ring with the Earth as Its Shepherd', Nature 337, 629.

Jewitt, D. C. and Danielson, G. E.: 1981, 'The Jovian Ring', J. Geophys. Res. 86, 8691.

Keller, H. U., Arpigny, C., Barbieri, C., Bonnet, R. M., Cazes, S., Coradini, M., Cosmovici, C. B., Delamare, W. A., Huebner, W. F., Hughes, D. W., Jamar, C., Malaise, D., Reitsema, H. J., Schmidt, H. U., Schmidt, W. K. H., Seige, P., Whipple, F. L., and Wilhelm, K.: 1986, 'First Halley Multicolour Camera Imaging Result from Giotto', Nature 321, 320.

Leinert, C., Richter, l., Pitz, E., and Planck, B.: 1981, 'The Zodiacal Light from 1.0 to 0.3 AU as Observed by the Helios Space Probes', Astron. Astrophys. 103, 177.

Leinert, C. and Grun, E.: 1990, in R. Schwenn and E. Marsch (eds.), 'Interplanetary Dust', Physics of the Inner Heliosphere, in the series Physics and Chemistry in Space, Springer-Verlag, Heidelberg, pp. 207-275.

McDonnell, J. A. M. (ed.): 1978, in 'Microparticle Studies by Space Instrumentation', Cosmic Dust, Wiley and Sons, Chichester, pp. 337-426.

Morfill, G. E., Grun, E., and Johnson, T. V.: 1980a, 'Dust in Jupiter's Magnetosphere: Physical Processes', Planetary Space Sci. 28, 1087.

Morfill, G. E., Grun, E., and Johnson, T. V.: 1980b, 'Dust in Jupiter's Magnetosphere: Origin of the Ring', Planetary Space Sci. 28, 1101.

Morfill, G. E., Grun, E., and Leinert, C.: 1986, in R. G. Marsden (ed.), 'The Interaction of Solid Particles with the Interplanetary Medium, The Sun and the Heliosphere in Three Dimensions, D. Reidel Publ. Co., Dordrecht, Holland, pp. 455-474.

Nagel, K., Neukum, G., Eichhorn, G., Fechtig, H., Muller, O., and Schneider, E.: 1975, 'Dependencies of Microcrater Formation on Impact Parameters', Proc. Lunar Sci. Conf. 6, 3417.

Nagel, K., Neukum, G., Dohnanyi, J. S., Fechtig, H., and Gentner, W.: 1976a, 'Density and Chemistry of Interplanetary Dust Particles Derived from Measurements of Lunar Microraters', Proc. Lunar Sci. Conf. 7, 1021.

Nagel, K., Neukum, G., Fechtig, H., and Gentner, W.: 1976b, 'Density and Composition of Interplanetary Dust Particles', Earth Planetary Sci. Letters 30, 234.

Opik, E.: 1951, 'Collision Probabilities with the Planets and the Distribution of Interplanetary Matter', Proc. Roy. Irish Acad. S4A, 165.

Owen, T., Danielson, G. E., Cook, A. F., Hansen, C., Hall, V. L., and Duxbury, T. C.: 1979, 'Jupiter's Rings', Nature 281, 442.

Rhee, J. W.: 1967, in J. C. Weinberg (ed.), 'Electrostatic Potential of a Cosmic Dust Particle', The Zodiaca/Light and the Interplanetary Medium, NASA SP-150, pp. 291-297.

Showalter, M. R., Cuzzi, J. N., and Pollack, J . B .: 1985, 'Discovery of Jupiter's Gossamer Ring', Nature 316, 526.

Showalter, M. R., Burns, J. A., Cuzzi, J. N., and Pollack, J. B.: 'Jupiter's Ring System: New Results on Structure and Particle Properties', Icarus 69, 458.

Smith, B. A., Soderblom, L. A., Beebe, R. F., Boyce, J., Briggs, G. A., Carr, M. H., Collins, S. A., Cook, A. F., II, Danielson, G. E., Davies, M. E., Hunt, G. E., Ingersoll, A. P., Johnson, T. V., Masursky, H., McCauley, J. F., Morrison, D., Owen, T., Sagan, C., Shoemaker, E. M., Strom, R. G., Suomi, V. E., and Veverka, J.: 1979a, 'The Galilean Satellites and Jupiter: Voyager 2 Imaging Science Results', Science 206, 927.

Smith, B. A., Soderblom, L. A., Johnson, T. V., Ingersoll, A. P., Shoemaker, E. M., Hunt, G. E., Masursky, H., Carr, M. H., Davies, M. E., Cook, A. F., II, Boyce, J., Danielson, G. E., Owen, T., Sagan, C., Beebe, R. F., Veverka, J., Strom, R. G., McCauley, J. F., Morrison, D., Briggs, G. A., and Suomi, V. E.: 1979b, 'The Jupiter System through the Eyes of Voyager 1', Science 204, 951.

Wyatt, S. P.: 1969, 'The Electrostatic Charge of Interplanetary Grains', Planetary Space Sci. 17, 155.

Zook, H. A. and Berg, O. E.: 1975, 'A Source for Hyperbolic Cosmic Dust Particles', Planetary Space Sci. 183, 183.

Zook, H. A., Lange, G., Grun, E., and Fechtig, H.: 1984, 'Lunar Primary and Secondary Microcraters and the Micrometeoroid Flux', Lunar and Planetary Science, Vol. XV, Houston, pp. 965-966.